Antifouling coatings for dental implants: PEG-like coatings on titanium by plasma polymerization

Judit Buxadera-Palomero[1,3,4], Cristina Canal[2,3,4], Sergi Torrent-Camarero[2,4], Beatriz Garrido[2,4], F. Javier Gil[2,3,4], Daniel Rodríguez[1,3,4*]

[1]Biomaterials, Biomechanics and Tissue Engineering Group, Department of Materials Science and Metallurgy, E. U. d'Enginyeria Tècnica Industrial de Barcelona, Technical University of Catalonia (UPC), C/ Comte d'Urgell 187, 08036 Barcelona, Spain

[2]Biomaterials, Biomechanics and Tissue Engineering Group, Department of Materials Science and Metallurgy, E. T. S. d'Enginyeria Industrial de Barcelona, Technical University of Catalonia (UPC), Av. Diagonal 647, 08028 Barcelona, Spain

[3]Biomedical Research Networking Centre in Bioengineering, Biomaterials, and Nanomedicine (CIBER-BBN), Maria de Luna 11, Ed. CEEI, 50118 Zaragoza

[4]Centre for Research in NanoEngineering (CRNE) – UPC, C/Pascual i Vila 15, 08028 Barcelona, Spain

*Corresponding author: daniel.rodriguez.rius@upc.edu

Abstract

Titanium dental implants are commonly used for the replacement of lost teeth, but they present a considerable number of failures due to the infection on surrounding tissues. The aim of this paper is the development of a polyethylene glycol-like (PEG-like) coating on the titanium surface by plasma polymerization to obtain a novel improved surface with suitable low bacterial adhesion and adequate cell response. Surface analysis data of these coatings are presented, in particular water contact angle, surface roughness and film chemistry, demonstrating the presence of a PEG-like coating. *S. sanguinis* and *L. salivarius* bacterial adhesion assays showed a decreased adhesion on the plasma polymerized samples, while cell adhesion of fibroblasts and osteoblasts on the treated surfaces was similar to control surfaces. Thus, the PEG-like antifouling coating obtained by plasma polymerization on Ti confers this biomaterial highly suitable properties for dental

1

applications, as they reduce the possibility of infection while allowing the tissue integration around the implant.

I. INTRODUCTION

In the last years, the use of dental implants has become increasingly common for overcoming the problematic of tooth loss [1]. Titanium and its alloys have been extensively used as raw materials for dental implants due to their excellent mechanical properties, low specific weight, high resistance to corrosion and high biocompatibility [2–5]. Despite their high rate of success, titanium dental implants still present a significant number of failures due to various factors e.g. absence of implant osseointegration, poor bone quality, smoking or infection. Among these factors, infection is thought to play an important role in the mid-long term failure of dental implants [1,6].

In a normal scenario, the presence of the periodontal ligament between tooth and gum isolates bone from the bacteria found in the mouth. The insertion of a dental implant destroys this ligament, leaving the surrounding bone exposed to infections if no biological sealing of gingival tissue with the implant surface is formed [7]. Therefore, the lack of a biological sealing in dental implants can compromise the success of the implant.

Bacteria can adhere on all hard surfaces in the oral cavity, i.e. teeth and dental implants, resulting in an implant-associated infection. Bacterial adhesion on the surface of implants leads to the formation of a biofilm, which is a sessile community embedded in an extracellular matrix produced by them. The biofilm is formed by a complex bacterial ecology, including early colonizers such as Streptococcus sanguinis [8–10], which attach to the surface and guide the later colonizers, such as Porphyromonas gingivalis, Fusobacterium nucleatum and Aggregabacter actinomycetemonitans [11,12]. Other species, such as Lactobacillus salivarius, have an important role on the formation and maintenance of the biofilm through the interaction with other strains and their by-products [13–15]. Once the bacteria have adhered on the surface, the host responds with a defense mechanism leading to inflammation of the soft tissues [16]. In the case of dental implants, this inflammation is called mucositis. Mucositis may develop into periimplantitis when plaque is accumulated for a prolonged period of time, affecting the periimplant supporting bone [17,18]. The prevalence of mucositis has been reported in some studies as 50% of the implanted sites, while periimplantitis was found in 28% of subjects [19] The treatment of infected implants is difficult, as most of the bacteria are in a stationary phase of growth

3

with low metabolism, which make them less susceptible to antibiotic therapy and nutrition deficiency. This infection is usually diagnosed at a late stage, when the surrounding tissue has been compromised. The consequences of the infection can result into intensive interventional medical and antibiotic therapies, loss of implant, impaired oral function, and even death. Thus, infection of a dental implant imposes significant health, emotional, and financial burdens to both patient and healthcare providers [2]. Debridement is the only option available, and when it fails, it is necessary to remove the implant [1,20–24]. The maturation of the biofilm causes resistance towards host immune response and antibiotic treatments. Thus, the best way to avoid the infection related with the implants is to avoid the initial adhesion of bacteria [2].

So far, extensive research has been focused on reducing the bacterial adhesion on the implant surface. Hence, antibacterial treatments for titanium implants can be broadly divided in three groups: incorporation of organic drugs, modification of the physical or chemical properties of the titanium surface and polymeric coatings.

Incorporation of drugs on the titanium surface can be carried out by direct adsorption on the titanium oxide layer or adsorbed in a coating. Different coatings have been investigated to immobilize antimicrobial agent such as biodegradable polymers, sol-gel coatings, nanotubes, hydroxyapatite or collagen [25–29]. The main types of antimicrobial agents that are used can be broadly classified as antibiotics, non-antibiotic antimicrobial agents and antimicrobial peptides. These treatments show good results in terms of bacterial adhesion decrease. However, the main drawbacks are biological safety concerns with some drugs, the development of bacterial resistance, especially against antibiotics, and a too fast drug release kinetics for dental applications [21].

Modification of the chemical and physical surface properties can be carried out by doping with antibacterial elements like silver [30,31], copper [32], fluorine [18], iodine [33] or zinc [34]. Modification of the crystalline structure of the titanium oxide surface layer has also shown antibacterial behavior [35–38]. Changes in the implant roughness can stimulate cell adhesion while reducing bacterial adhesion [39,40].

4

The principle behind polymeric antibacterial coatings design is to either repel the microbes or kill them on contact. Depending on the interaction with bacteria the coating can be biopassive (repelling the bacteria) or bioactive (killing the bacteria) [41,42]. Polymers used as antibacterial coatings are either cationic (bioactive) or non-charged hydrophilic or hydrophobic polymers (biopassive).

One of the best known antifouling polymers is poly(ethylene glycol) (PEG) [43]. PEG chains are believed to resist protein adsorption via two mechanisms: steric repulsion due to chain compression and by acting as a barrier created by structured water associated with the PE G[44–46]. Many different approaches have been used to immobilize PEG on the biomaterials surface: self-assembly, physisorption, silanization, electropolymerization or plasma polymerization among others [2,47–50]. However, plasma polymerization to obtain PEG-like coatings has been extensively used on polymeric surfaces[50–55] but, to the best of our knowledge, not on titanium surfaces.

Glow discharge plasma treatment is frequently used for cleaning, preparation, and modification of biomaterial and implant surfaces [56]. One of the processes achieved by glow discharge plasmas is plasma polymerization, in which an organic precursor is introduced in the reaction chamber in order to obtain nanometer-thin coatings on the implant surface. By modifying the process parameters and the precursor molecule, different kinds of biocompatible coatings can be produced, from cell-adhesive coatings to antifouling coatings.

The aim of this work was to evaluate the possibility of obtaining polyethylene glycol-like (PEG-like) coatings on the titanium surface by plasma polymerization to generate improved surfaces with suitable low bacterial adhesion and adequate cell response. The plasma polymerization process was performed with tetra(ethylene glycol) dimethyl ether (Tetraglyme) on titanium through a two-step process: plasma activation followed by plasma polymerization. Parameters like power and time for plasma activation of titanium were studied in terms of wettability and surface chemistry to optimize the conditions. The influence of power and time on the plasma polymerization process was

5

evaluated for the polymerization. The properties of the coatings were analyzed by water contact angle, FTIR, XPS, SEM, cytotoxicity and cell and bacterial adhesion.

II. EXPERIMENTAL SET UP AND METHODOLOGY

A. Materials

Rods of commercially pure titanium grade 2 were machined to produce disks of 10 mm diameter and 2 mm thickness. These disks were used as a substrate for all samples. The surface of the disks were grinded with silicon carbide wet grinding paper (P600, P800, P1200 and P2500, Buehler, USA) and polished in a subsequent stage with a colloidal silica suspension (0.05 µm size, Buehler, USA). Polished samples were cleaned with a sequence of organic solvents: toluene, isopropanol, water, ethanol and acetone (Sigma Aldrich, USA) in an ultrasonic bath for 15 min each. Samples treated up to this stage were used as control group (Ti). Tetraethylene glycol dimethyl ether (tetraglyme) (Sigma Aldrich, USA) was used as received.

B. Low pressure plasma treatments

Ti disks were treated with low pressure plasma in a 13.52 MHz radiofrequency commercial reactor "Diener Femto" (Diener, Germany) composed of a quartz chamber with a volume of 2 l. For treatments, 5 samples were laid horizontally on a quartz tray in the centre of the reactor (**Figure 1**).
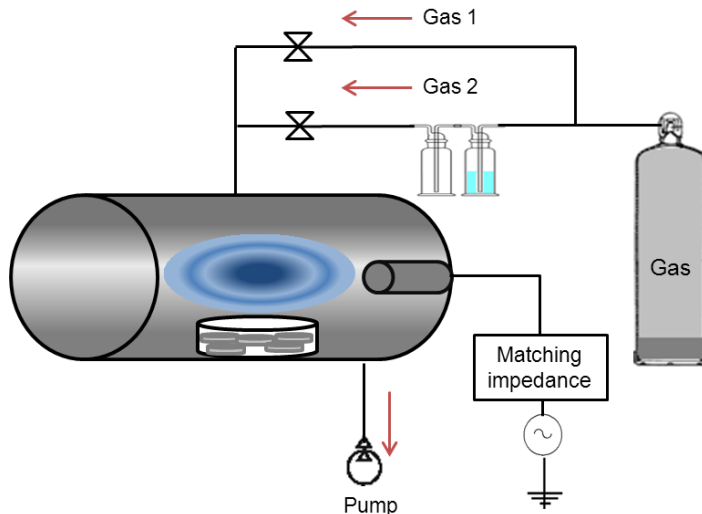
Figure 1. Configuration of the plasma system used for the study

1. *Plasma activation*

In a first step, Ti samples were plasma-treated with non-polymerizing gases for surface activation. To ascertain the most suitable treatment for activation of Ti, different conditions were tested in continuous wave (CW) plasma mode, at 0.40 mbar, and using different plasma gases, treatment times and discharge powers, as detailed in table I.

Table I. Plasma parameters employed in the activation treatments of titanium. Sample codes used in the paper are indicated

Gas	Power (W)	Time of treatment (min)	Sample code
Oxygen	100	0.5	O_2PA100_05
Oxygen	100	2	O_2PA100_2
Oxygen	100	5	O_2PA100_5
Oxygen	100	0.5	O_2PA200_05
Oxygen	100	2	O_2PA200_2
Oxygen	100	5	O_2PA200_5
Argon	200	0.5	ArPA200_05
Argon	200	2	ArPA200_2
Argon	200	5	ArPA200_5
Argon	200	0.5	ArPA200_05
Argon	200	2	ArPA200_2
Argon	200	5	ArPA200_5

2. Plasma polymerization

Plasma polymerization treatments were performed by using Argon (Ar) as carrier gas, which was bubbled through the monomer tetraglyme after the plasma activation treatment. Pulsed power was employed to perform the polymerization treatments, with a duty cycle of 0.1% at a pulse-on time of 20 µs and pulse-off of 20 ms. Pressure was kept at 0.40 mbar during treatments, and different conditions were evaluated to produce the coatings (table II).

Table II. Plasma parameters employed in the plasma polymerization treatments. Sample codes used in the paper are indicated.

Peak power (W)	Time of treatment (min)	Sample code
100	30	PP100_30
100	60	PP100_60
150	30	PP150_30
150	60	PP150_60
200	30	PP200_30
200	60	PP200_60

C. Wettability

Surface wettability was determined by the sessile-drop method using an OCA15 (Dataphysics instrument Company, Germany) equipment with ultra-pure MilliQ (Millipore Corporation) water. A 2 µl droplet of water was deposited at 1 µl/s on the surface of the studied specimens. The drop image was captured by a video camera and analyzed using the SCA20 software (Dataphysics instrument Company, Germany). Three measurements were carried out on three different samples for each condition.

D. Chemical characterization

Fourier Transformed Infrared Spectra were recorded using a FTIR Nicolet 6700 in the transmittance mode, (128 scans and resolution 1 with data spacing 0.482 cm^{-1}). Potassium Bromide (KBr) disks were used as the substrate for plasma polymerization instead of Ti for the FTIR measurements.

X-ray photoelectron spectroscopy (XPS) was acquired in ultra-high vacuum ($5.0 \cdot 10^{-9}$ mbar) with an XR50 Mg anode source operating at 150 W and a Phoibos 150

8

MCD-9 detector (D8 advance, SPECS Surface Nano Analysis GmbH, Germany). Spectra were recorded at pass energy of 25 eV with a stepsize of 1.0 eV for survey spectra and 0.1 eV for high resolution spectra. The recorded core levels were C 1s, O 1s and Ti 2p. C 1s peak was used as a reference. CasaXPS software (Casa Software Ldt, UK) was used for the determination of atomic elemental composition applying the manufacturer set of relative sensitivity factors.

E. *Topography characterization*

Surface topography of the samples was observed with a Zeiss Neon40 Scanning Electron Microscope (SEM Carl Zeiss NTS GmbH, Jena, Germany). Images of titanium and plasma polymerized titanium samples were taken with secondary electrons at working distance of 7 mm and accelerating voltage of 5 kV.

Surface roughness was measured with the optical profiling system WYKO NT1100 and WYKO Vision 232[TM] software (Veeco Instruments, Plainview, NY, USA) in vertical scanning interferometry (VSI) mode. The area analyzed was 736 µm x 480 µm for all samples. Three measurements were performed in three samples for each condition, computing the arithmetic average height (R_a).

F. *Biological characterization*

1. *Cytotoxicity*

Potential cytotoxic effects of the plasma-coated Ti were evaluated according to ISO 10993-5 standard on human foreskin fibroblasts (hFFs, Merck Millipore Corporation, Bedford, MA, USA) and human osteosarcoma cell line (SAOS-2, ATCC, USA), using three samples for each condition. All specimens were sterilized by immersion in ethanol 70% during 30min. Extracts of the samples at concentrations of 1:1, 1:10, 1:100 and 1:1000 were prepared by immersing the samples in Dulbecco's Modified Eagle Medium (DMEM, Invitrogen, Carlsbad, CA, USA) for the hFFs and McCoy's (Invitrogen, Carlsbad, CA, USA) for SAOS-2 at 37 °C for 72 h. 5000 cells/well were seeded on a 96-well tissue polystyrene (TCPS) dish and incubated with media for 24 h. Afterwards, culture media were replaced by the extract dilutions. After 24 h, cells were lysed with mammalian protein

extraction reagent (mPER, Thermo Scientific, USA) and cell viability was measured by the activity of the enzyme lactate dehydrogenase (LDH) with a Cytotoxity Detection Kit (Thermo Scientific, USA). Cells seeded in the TCPS were used as the positive control, and culture media was used as the negative control. The cell viability was calculated following the equation 1, were Abs is the measured absorbance for the samples (Abs_{sample}) and the positive (Abs_{C+}) and negative control (Abs_{C-}).

$$cell\ viability = (Abs_{sample} - Abs_{C-}/(Abs_{C+} - Abs_{C-}) \qquad \text{Equation 1}$$

2. Protein adsorption

Protein adsorption on the Ti surface was tested by immersing the samples in bovine serum albumin (BSA, Sigma Aldrich, USA). BSA was stained with Fluorescein Isotiocianate (FITC) with the Kit Pierce Antibody Labeling Kit (Thermo Scientific, USA). The staining was performed by dissolving BSA in a phosphate-borate buffer, mixed with a FITC solution and purified in a resin to remove the non-reacted FITC. Samples were then immersed in 150 µl of FITC-BSA at a concentration of 100 µg/ml during 1 h in darkness. Protein was fixed with paraformaldehyde (Sigma Aldrich, USA). After each step samples were washed with phosphate buffer saline (PBS). Coverslips were mounted on the samples in Mowiol (Merck Millipore Corporation, Bedford, MA, USA) mounting medium. Samples were photographed with a Nikon E-600 fluorescence microscope, and an Olympus DP72 camera (Nikon Corporation Instruments Company, USA). To assess the protein adsorption, four images were taken for each sample and the pixel intensity was calculated by the software Image-J (NIH, MD, USA).

3. Cell adhesion

Cell adhesion was studied by seeding $2 \cdot 10^4$ cells on triplicate specimens, and incubated for 6 h in a 48-well culture plate. Ti and the culture dish (TCPS) were used as controls. Cells used were hFFs and SAOS-2. Cell numbers were assessed with the Cytotoxity Detection Kit (LDH).

Specimens were prepared for SEM by fixing the cells with 4% paraformaldehyde in PBS, and a sequence for dehydrating the cells was performed by immersing the samples

10

in 50%, 70%, 90%, 96% and 100% (v/v) ethanol during 15 min each step. As the final step, samples were immersed in HDMS overnight and carbon coated.

4. Bacterial adhesion

Bacterial adhesion assays were performed with two oral bacterial strains: Streptococcus sanguinis (*S. sanguinis* CECT 480, Colección Española de Cultivos Tipo (CECT), Valencia, Spain) and Lactobacillus salivarius (*L. salivarius* CCUG 17826, Culture Collection University of Göteborg (CCUG), Göteborg, Sweden). *S. sanguinis* was grown and maintained in Todd-Hewitt (TH) broth (Scharlab SL, Spain) and *L. salivarius* in MRS broth (Scharlab SL, Spain). Cultures were incubated overnight at 37 °C before each assay. The optical density of each bacterial suspension was adjusted to 0.2 ± 0.01 at 600 nm, giving approximately $1 \cdot 10^8$ colony-forming units (CFU)/ml for each strain.

Samples were immersed in 1 ml of bacterial suspension ($1 \cdot 10^8$ CFU/ml) for 2 h at 37 °C. After this time, the medium was suctioned and samples were washed twice with PBS (Gibco, UK). Adherent bacteria were detached by vortexing the disks for 5 min in 1 ml of PBS. Detached bacteria were then seeded using serial dilutions on TH agar plates for *S. sanguinis* and MRS agar plates for *L. salivarius*. The plates were then incubated at 37 °C for 24 h and the resulting colonies counted. Three samples for each condition were studied and two different dilutions of each sample were seeded in different agar plates.

5. Statistical analysis

The data were analyzed using Student's t-tests and one-way ANOVA tables with Tukey's multiple comparison tests in order to evaluate statistically significant differences between sample groups. The differences were considered to be statistically significant when $p<0.05$. All statistical analyses were performed with Minitab 16™ software (Minitab, Inc., State College, PA).

11

III. RESULTS

A. *Plasma activation*

Wettability of the samples increased with all the plasma activation (PA) treatments with non-polymerizing gases at different powers from an initial value of water contact angle of 57º for the Ti to a superhydrophilic surface (below 5º) (Figure 2a). The best wettability was obtained for the argon activation at 100 W (ArPA100_5), as these samples have the lowest water contact angle.

XPS analysis of Ti reveals the presence of oxygen, which account for the presence of titanium oxide and of carbon, which may come from adsorbed contaminants on the surface. The XPS of the PA samples was performed on two of the studied conditions: O_2PA200_5 and ArPA100_5. In both conditions, a decrease of the carbon amount on the titanium surface can be observed comparing the untreated Ti to the plasma activated one (Table III) due to the cleaning effect of the treatment. As a consequence of the lower attenuation, the titanium and oxygen signals are higher and more intense, yielding higher atomic concentration. Differences between the O_2PA200_5 and the ArPA100_5 are not statistically significant. Following the results on wettability and XPS, the condition selected for further work for the titanium activation was ArPA100_5.

Table III. Atomic concentration (in %) of the carbon, oxygen and titanium amount present on the Ti, O_2PA200_5 and ArPA100_5

	C 1s	O 1s	Ti 2p
Ti	23 ± 2	59 ± 1	18 ± 1
O_2PA200_5	13 ± 2	64 ± 1	23 ± 1
ArPA100_5	15 ± 1	62 ± 1	22 ± 1

B. *Plasma polymerization: process characterization*

Water contact angle of plasma polymerized (PP) samples showed an increase in all cases with respect to the activated sample (figure 2b), while roughness was kept unaltered (from a R_a value of 45 ± 5 nm before the polymerization to a value of 46 ± 4 nm). No changes could be either observed on the topography of the samples with the SEM images (Figure 3).

12
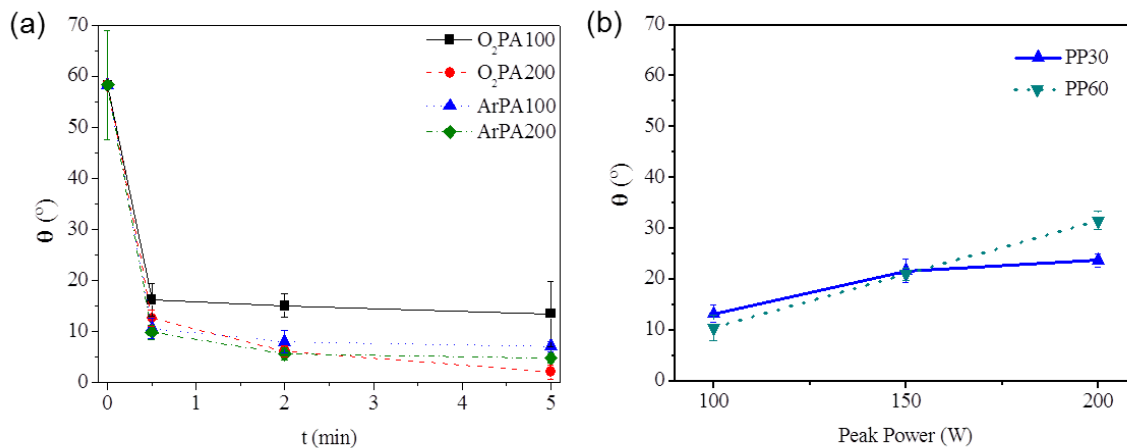
Figure 2. Water contact angle of the PA samples (a) and the PA+PP samples (b)
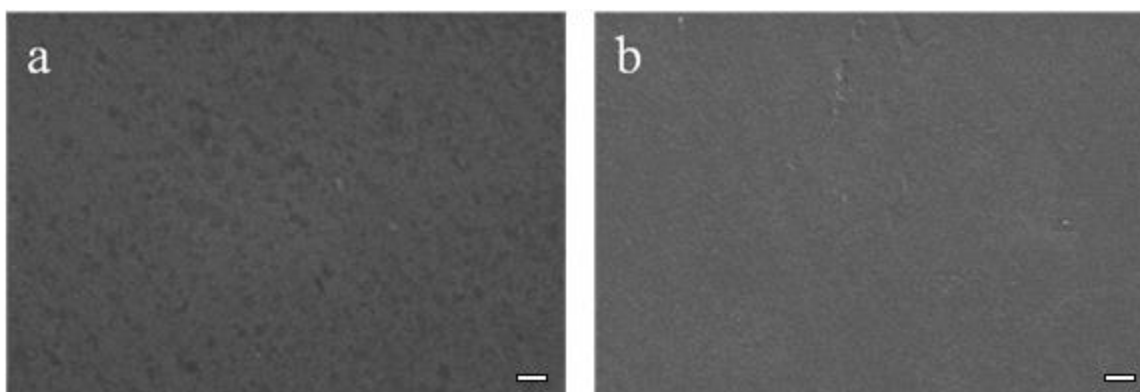
Figure 3. SEM image of Ti (a) and PP100_1 (b). Scale bar indicates 2 μm

Chemical composition of the samples was assessed by FTIR and XPS. FTIR spectra (Figure 4) show the characteristic peaks for a PEG-like coating obtained by plasma polymerization. Comparing the spectra of PP coatings on Ti with the spectra of commercial PEG can be observed the presence of the same peaks (table IV). No differences between different PP treatment conditions were observed (data not shown).
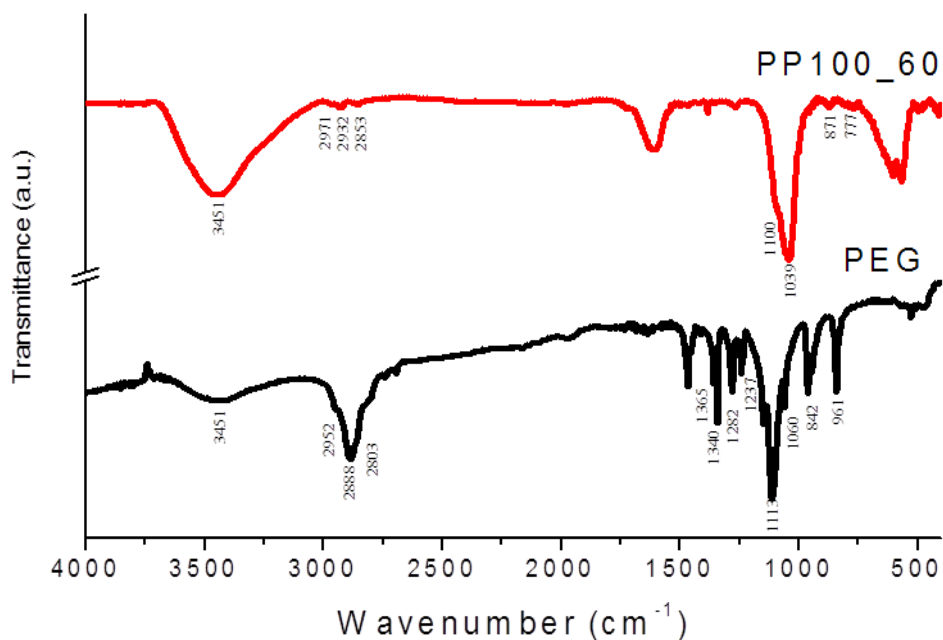
Figure 4. FTIR spectra of the reference PEG and PP100_60. Two main peaks can be observed, st(C-O) at 1100cm-1 and st(C-H) at 2950cm-1.

Table IV. Band assignation for the reference PEG and the PEG obtained by plasma polymerization.

	PEG ν (cm^{-1})	PEG coating ν (cm^{-1})
C-H in plane bending	842, 961	777, 871
C-O-C stretching	1060, 1113	1039, 1100
C-C stretching	1237, 1282, 1340, 1365	
C-H stretching	2803, 2888, 2952	2853, 2932, 2971
O-H stretching	3451	3451

The atomic concentration of the elements in the outer surface was recorded by XPS and is summarized in table V. When comparing the PP samples with the PA ones, an increase of the intensity for the carbon peak can be observed while the titanium peak decreases. The increase on the C/Ti ratio reflects the formation of a PEG-like coating on the surface, which was further confirmed by the high-resolution decomposition of the carbon peak (table VI).

**Table V. Atomic concentration (in %) of carbon, oxygen and titanium obtained by XPS, and C/Ti ratio**

14

	C 1s	O 1s	Ti 2p	C/Ti
Ti	23 ± 2	59 ± 1	18 ± 1	1 ± 0
ArPA100_5	15 ± 1	62 ± 1	22 ± 1	1 ± 0
PP100_30	40 ± 14	46 ± 10	14 ± 4	2 ± 0
PP100_60	38 ± 0	52 ± 1	10 ± 1	4 ± 0
PP150_30	48 ± 1	44 ± 1	7 ± 1	7 ± 1
PP150_60	50 ± 1	43 ± 1	5 ± 1	10 ± 0
PP200_30	45 ± 1	46 ± 0	8 ± 1	6 ± 0
PP200_60	53 ± 1	41 ± 1	5 ± 0	10 ± 0

In the decomposition of the carbon peak (table VI), four different peaks were found, corresponding respectively with the hydrocarbon bonds (C-H, C-C) at 284.8 eV, the ether bonds (C-O-C) at 286.5 eV, the carboxyl bonds (O-C-O) at 288 eV and the carboxylic bonds (O-C=O) at 289 eV. The peak at 286.5 eV is the most characteristic of PEG as it is associated with the ether bond. This peak showed a decrease when increasing the power and the time of polymerization. The peaks at 288 eV and 289 eV are consequence of the fragmentation of the polymer during the polymerization.

Table VI. Components (in atomic %) of the C 1s peak according to the carbon environment in the coated samples

	C-H, C-C	C-O-C	O-C-O	O-C=O
ArPA5_100	66 ± 3	28 ± 2	-	7 ± 1
PP100_30	1 ± 2	67 ± 4	21 ± 2	11 ± 3
PP100_60	14 ± 2	59 ± 2	12 ± 3	15 ± 3
PP150_30	24 ± 11	46 ± 3	25 ± 13	6 ± 2
PP150_60	18 ± 2	41 ± 1	32 ± 2	8 ± 1
PP200_30	14 ± 1	48 ± 3	32 ± 3	6 ± 1
PP200_60	21 ± 8	44 ± 1	29 ± 8	7 ± 1

Comparing the XPS spectra of C 1s of the steps used in the process (figure 5), it can be observed that the main peak observed in the Ti samples and the PA samples is the C-H peak at 285 eV, while for the plasma polymerized samples the main peak is the C-O peak at 286.5 eV.

15
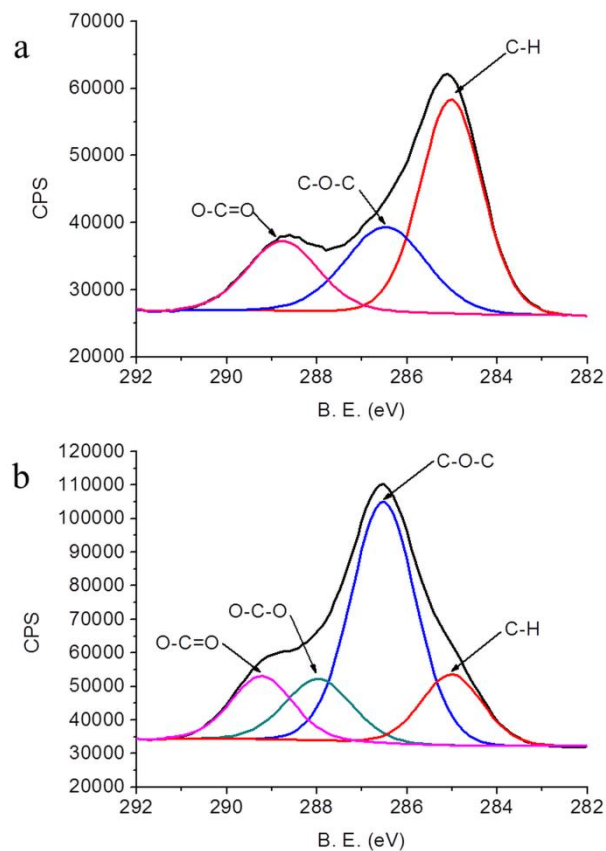
Figure 5. High resolution C 1s XPS spectra for ArPA100_5 (a) and PP100_60 (b). The peaks corresponding to the carbon decomposition are indicated in the figure

C. Plasma polymerization: biological performance

1. Cytotoxicity

Cell viability showed no decrease at any dilution when tested with fibroblasts and osteoblasts (Figure 6). All the studied surfaces and the plasma polymerization conditions had cell viability ratios over 80%, showing the good biocompatibility of the coatings.

16
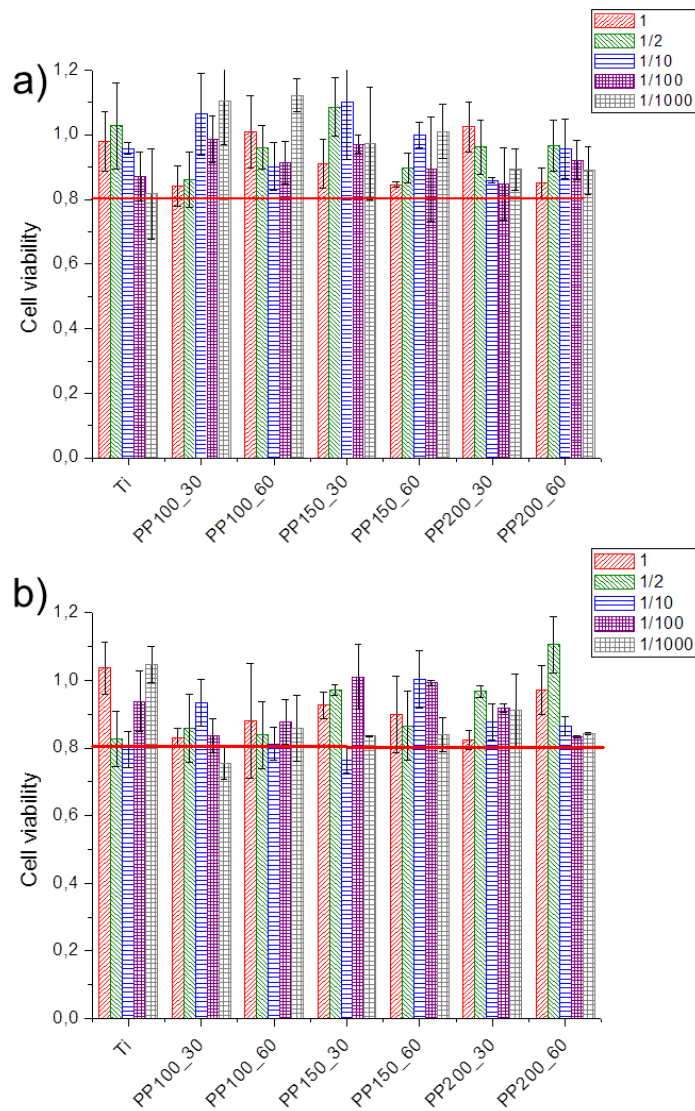
Figure 6. Cell viability of the hFFs (a) and the SAOS-2 (b)

2. *Protein adsorption*

Protein adsorption with BSA was tested in fluorescence assays (Figure 7) Fluorescence intensity is an indicator of the protein presence, as FTIC molecules are bonded to the BSA. Certain plasma polymerization conditions showed lower protein adsorption than Ti (PP100_60, PP150_60 and PP200_60).
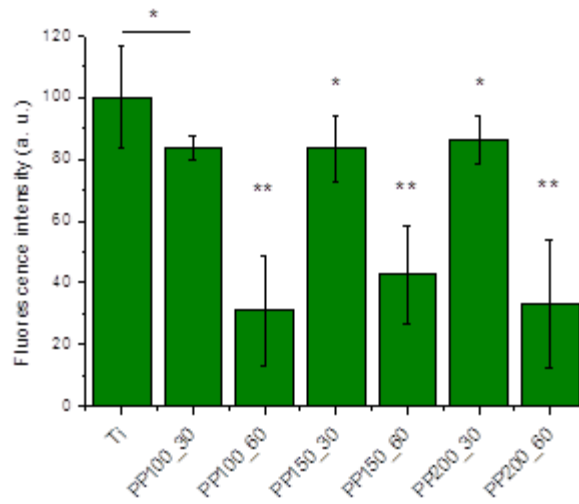
Figure 7. Fluorescence intensity detected for the different samples. Bars indicated with the same symbol have no statistically significant difference between them (p>0.05).

3. Bacterial adhesion

Bacterial adhesion assays showed a decreased bacterial adhesion for all PP samples either for the *S. sanguinis* and the *L. salivarius* (Figure 8). Ti samples and plasma activated samples ArPA100_5 were used as controls. An increased bacterial adhesion was observed for the PA sample compared to Ti.
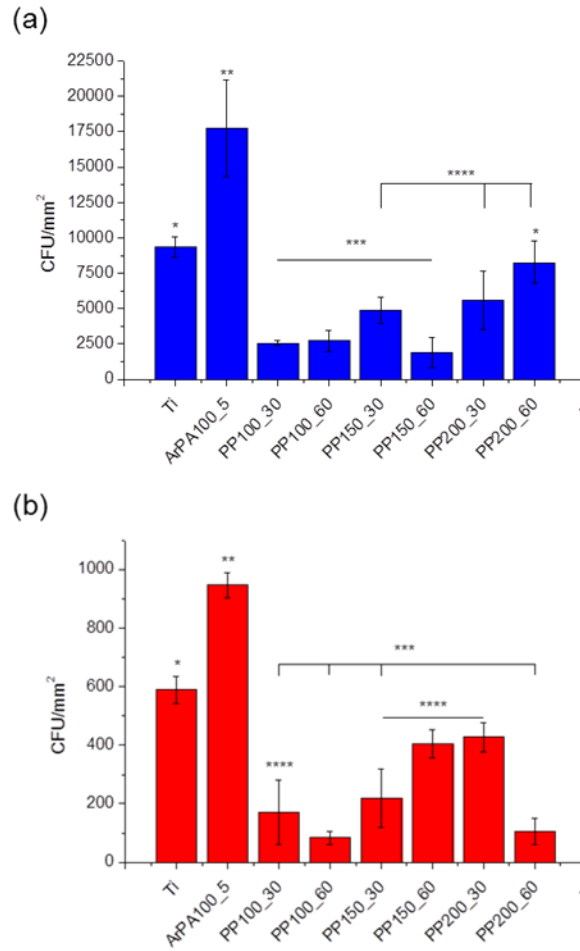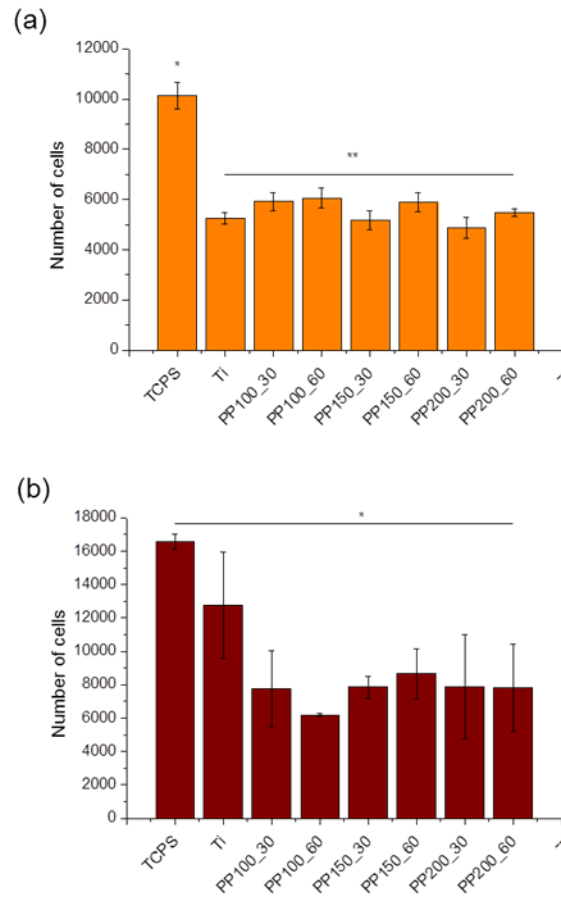
18

(a)

(b)

Figure 8. Bacterial adhesion on Ti, PA and PP samples of *S. sanguinis* (a) and *L. salivarius* (b). Bars indicated with the same symbol have no statistically significant difference between them (p>0.05)

4.   Cell adhesion

Cell adhesion assays with hFFs (Figure 9(a)) showed no difference between Ti and PP samples, while for SAOS-2 (Figure 9(b)) a slightly decrease was measured. In terms of cell morphology (Figure 10), no differences are observed in any of the cell lines studied.

Figure 9. Cell adhesion of hFFs (a) and SAOS-2 (b) on the Ti and PP samples. Bars indicated with the same symbol have no statistically significant difference between them (p<0.05)
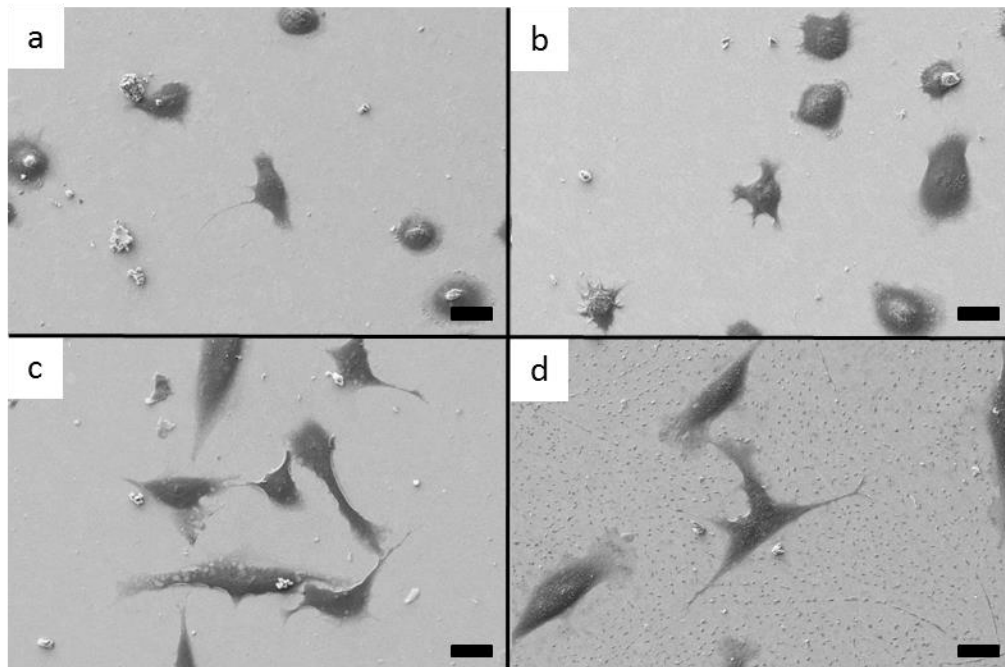
Figure 10. SEM images of the cell adhesion on the Ti and a PP sample. (a) SAOS-2 on Ti, (b) SAOS-2 on PP100_60, (c) hFFs on Ti, (d) hFFs on PP100_60

IV. DISCUSSION

A. *Plasma activation*

Activation of titanium is an important step for its chemical functionalization, as titanium is naturally covered by a titanium oxide layer with low chemical reactivity [57,58]. As shown by XPS (table III), plasma activation has two main effects on the titanium surface, as it cleans the surface from organic contaminants (hydrocarbons) [59,60], and it produces a reactive surface which can be then used in a subsequent step for the bonding with a polymeric layer [56,57,61]. This treatment renders a higher hydrophilicity, as shown by the water contact angle measurements (figure 2a). The cleaning and activation process was followed by water contact angle, where it can be observed that all the different plasma activation conditions tested yield a water contact angle lower than that of untreated Ti (figure 2), from a value of 58.3º ± 10 to values below 5º. Oxygen and argon were evaluated for activation, and argon showed to be more effective. In the argon activation, the effect of the applied power was less pronounced than in the case of oxygen activation. This fact can be explained by the differences in the breakdown potential of the two gases. As argon has a lower breakdown voltage than oxygen, the plasma dissociation is easier and the number of active species is higher, so the enhanced activation can be achieved with Ar at lower plasma powers [62–65].

B. *Plasma polymerization: process characterization*

Contact angle of the plasma polymerized samples (Figure 2b) showed the hydrophilic character of the PEG-like coating, with water contact angles ranging between 10-30º. The values obtained are slightly lower than the ones found in the literature [43,58,66–68].

FTIR spectra of the plasma polymerized samples display the typical bands for the PEG-like samples, as assigned in previous studies [68,51,69,54]. Band assignation for the reference PEG (PEG) and the plasma polymerized sample (PEG coating) is summarized in table IV, where C-O-C ether bonds characteristic of PEG and OH terminal groups can be identified. No differences were found when comparing the spectra for the different plasma polymerization conditions.

22

Some of the bands were absent or reduced in intensity compared to the reference PEG. This indicates the possibility of cross-linking for the plasma polymerized coating, with changes in the C-H bands, through the reduction of the C-H stretching bands and the C-C stretching bands. The cross-linking is a good tool for decreasing the solubility of the PP-PEG layers [51,70] (Figure 4).

XPS results (Table V) showed an increase in the carbon amount due to the deposition of the PEG-like coating on the surface [44,45]. This is a consequence of attenuation of the substrate photoelectrons by the polymeric coating [71]. The C/Ti ratio is a good indicator of the thickness of the coating [72], so a higher amount of PEG-like coating can be detected for the samples polymerized at 150W and 200W (PP150_60 and PP200_60). At constant treatment power, a higher amount of PEG can be observed for the samples polymerized at 1h. From these results, it can be concluded that the higher the power and time of polymerization, the thicker the coating obtained.

Due to the PEG chemical structure, the carbon peak can be decomposed in four peaks, for the different chemical environments found in a PEG-like coating, i.e., hydrocarbons (C-C or C-H), ether (C-O-C), carbonyl groups (C=O) and carboxylic groups (O-C=O). PEG have a XPS spectra with one peak at 286.5 eV, showing the presence of ether bonding and another peak at 285 eV, corresponding to the C-C bonds [73]. Thus, the ether peak is indicative of the PEG character of the coating, and can be related to the fragmentation process during the plasma polymerization. The coatings with the higher ether peak were the ones obtained at 100W (PP100_30 and PP100_60), showing the lower fragmentation of the precursor at lower powers [47,74,52].

C. *Plasma polymerization: biological performance*

PEG coatings for biomedical devices are intended to be non-toxic, antifouling and to show a decrease on the bacterial and cell adhesion.

The antifouling effect of the deposited coatings on Ti was studied by the fluorescence staining of BSA, with a reduction of the protein adsorption in all the cases. The thicker coatings obtained by polymerization during 1h clearly led to lower protein adsorption. This, in conjunction with the fact that all the plasma polymerization conditions

23

rendered a lower bacterial adhesion was a very interesting result for the antifouling performance of the obtained coatings [75,76]. The surfaces processed at lower powers had a better performance in terms of the bacterial adhesion. These results are in agreement with the XPS results, showing that a higher ether character (peak at 286.5eV) and thus more PP-PEG produces a coating with less bacterial adhesion [74,77–79,53].

The biocompatibility of the coating was studied with cytotoxicity assay and cell adhesion assays. The lixiviates eluted by the plasma polymerized coatings obtained at the studied conditions did not show any toxicity (Figure 5), as the cell viability overcomes the 80% in all cases, and most generally over 90%. In terms of the cell adhesion, both osteoblasts and fibroblasts were studied and no statistically significant differences were observed between the PP Ti samples and the Ti, and the cell morphology observed by SEM images (Figure 9) was similar for all the samples. Although this result is surprising, the parameters used for the plasma polymerization can lead to these results, because the use of higher powers can lead to surfaces with a good cell adhesion [52,75,76]. Considering the application of the PEG-like coating on titanium for dental implants, this kind of coatings can lead to a biocompatible and integrated implant with a lower incidence of infections.

Among the different plasma coatings produced on Ti, the one which has shown better performance for the use in dental implants is the PP100_60 (polymerization at 100W during 1h), as it has a good cellular adhesion, and a significant decrease of the protein adsorption and cellular adhesion.

V. SUMMARY AND CONCLUSIONS

In the design of dental implants, bacterial colonization and lack of biological sealing can compromise their success. In the present work, novel titanium biomaterial surfaces have been designed by PEG-like plasma polymerization with views on conferring them antifouling and low bacterial adhesion properties while maintaining adequate cell adhesion. Prior to polymerization titanium was activated with non-polymerizing gases, of which, an Argon plasma treatment at 100W and 5 min showed optimum results, rendering

superhydrophilic surface properties and a higher amount of reactive groups, suitable for subsequent reaction with the plasma polymer. The plasma polymerization coatings obtained from Tetraglyme in different treatment conditions were hydrophilic (θ=10-30°), they did not modify the topography of the samples and their chemical characteristics observed by FTIR and XPS correspond to PEG coatings. The *in vitro* results show that PEG-like coatings are appropriate for the use on dental implants, as they decreased the *S. sanguinis* and *L. salivarius* bacterial adhesion and showed antifouling properties without significantly altering significant the hFFs and SAOS-2 cell adhesion.

ACKNOWLEDGMENTS

1. A. D. Pye, D. E. A. Lockhart, M. P. Dawson, C. A. Murray, and A. J. Smith, J. Hosp. Infect. **72**, 104 (2009).

2. K. Subramani and R. T. Mathew, *Emerging Nanotechnologies in Dentistry* (Elsevier, 2012), pp. 85–102.

3. C. Larsson, P. Thomsen, B. O. Aronsson, M. Rodahl, J. Lausmaa, B. Kasemo, and L. E. Ericson, Biomaterials **17**, 605 (1996).

4. P. Tengvall and I. Lundström, Clin. Mater. **9**, 115 (1992).

5. H. F. Morris, S. Winkler, and S. Ochi, J. Oral Implantol. **27**, 180 (2001).

6. I. K. Karoussis, U. Brägger, G. E. Salvi, W. Bürgin, and N. P. Lang, Clin. Oral Implants Res. **15**, 8 (2004).

7. T. Berglundh, J. Lindhe, I. Ericsson, C. P. Marinello, B. Liljenberg, and P. Thornsen, Clin. Oral Implants Res. **2**, 81 (1991).

8. P. E. Kolenbrander, R. N. Andersen, and L. V. H. Moore, Appl. Environ. Microbiol. **56**, 3890 (1990).

9. M. Godoy-Gallardo, C. Mas-Moruno, M. C. Fernández-Calderón, C. Pérez-Giraldo, J. M. Manero, F. Albericio, F. J. Gil, and D. Rodríguez, Acta Biomater. **10**, 3522 (2014).

10. K. Hori and S. Matsumoto, Biochem. Eng. J. **48**, 424 (2010).

11. P. E. Kolenbrander and J. London, J. Bacteriol. **175**, 3247 (1993).

12. G. Mayanagi, T. Sato, H. Shimauchi, and N. Takahashi, Int. Congr. Ser. **1284**, 195 (2005).

13. L. C. Pham, R. J. M. van Spanning, W. F. M. Röling, A. C. Prosperi, Z. Terefework, J. M. Ten Cate, W. Crielaard, and E. Zaura, Arch. Oral Biol. **54**, 132 (2009).

14. S. Harder, R. Podschun, L. Grancicova, C. Mehl, and M. Kern, Clin. Oral Investig. **17**, 1135 (2013).

15. A. Almståhl, M. Wikström, and B. Fagerberg-Mohlin, Oral Dis. **14**, 541 (2008).

16. M. M. Fürst, G. E. Salvi, N. P. Lang, and G. R. Persson, Clin. Oral Implants Res. **18**, 501 (2007).

17. D. Dufour, V. Leung, and C. M. Lévesque, Endod. Top. **22**, 2 (2010).

18. M. Yoshinari, Y. Oda, T. Kato, and K. Okuda, Biomaterials **22**, 2043 (2001).

19. H. Algraffee, F. Borumandi, and L. Cascarini, Br. J. Oral Maxillofac. Surg. **50**, 689 (2012).

20. P. A. Norowski and J. D. Bumgardner, J. Biomed. Mater. Res. B. Appl. Biomater. **88**, 530 (2009).

21. L. Zhao, P. K. Chu, Y. Zhang, and Z. Wu, J. Biomed. Mater. Res. B. Appl. Biomater. **91**, 470 (2009).

22. N. Hadjesfandiari, K. Yu, Y. Mei, and J. N. Kizhakkedathu, J. Mater. Chem. B **2**, 4968 (2014).

23. J. Mouhyi, D. M. Dohan Ehrenfest, and T. Albrektsson, Clin. Implant Dent. Relat. Res. **14**, 170 (2012).

24. E. M. Hetrick and M. H. Schoenfisch, Chem. Soc. Rev. **35**, 780 (2006).

25. M. Lucke, G. Schmidmaier, S. Sadoni, B. Wildemann, R. Schiller, N. P. Haas, and M. Raschke, Bone **32**, 521 (2003).

26. K. C. Popat, L. Leoni, C. A. Grimes, and T. A. Desai, Biomaterials **28**, 3188 (2007).

27. K. C. Popat, M. Eltgroth, T. J. Latempa, C. A. Grimes, and T. A. Desai, Biomaterials **28**, 4880 (2007).

28. S. Radin and P. Ducheyne, Biomaterials **28**, 1721 (2007).

29. A. A. Campbell, L. Song, X. S. Li, B. J. Nelson, C. Bottoni, D. E. Brooks, and E. S. DeJong, J. Biomed. Mater. Res. **53**, 400 (2000).

30. M. Godoy-Gallardo, A. G. Rodríguez-Hernández, L. M. Delgado, J. M. Manero, F. Javier Gil, and D. Rodríguez, Clin. Oral Implants Res. (2014).

31. D.-H. Song, S.-H. Uhm, S.-B. Lee, J.-G. Han, and K.-N. Kim, Thin Solid Films **519**, 7079 (2011).

32. E. A. A. Neel, I. Ahmed, J. Pratten, S. N. Nazhat, and J. C. Knowles, Biomaterials **26**, 2247 (2005).

33. H. Tsuchiya, T. Shirai, H. Nishida, H. Murakami, T. Kabata, N. Yamamoto, K. Watanabe, and J. Nakase, J. Orthop. Sci. **17**, 595 (2012).

34. H. Hu, W. Zhang, Y. Qiao, X. Jiang, X. Liu, and C. Ding, Acta Biomater. **8**, 904 (2012).

35. P. Petrini, C. R. Arciola, I. Pezzali, S. Bozzini, L. Montanaro, M. C. Tanzi, P. Speziale, and L. Visai, Int. J. Artif. Organs **29**, 434 (2006).

36. B. Del Curto, M. F. Brunella, C. Giordano, M. P. Pedeferri, V. Valtulina, L. Visai, and A. Cigada, Int. J. Artif. Organs **28**, 718 (2005).

37. L.-H. Nie, C. Shi, Y. Xu, Q.-H. Wu, and A.-M. Zhu, Plasma Process. Polym. **4**, 574 (2007).

38. B. Wälivaara, B.-O. Aronsson, M. Rodahl, J. Lausmaa, and P. Tengvall, Biomaterials **15**, 827 (1994).

39. P. F. Amoroso, A. Pier-Francesco, R. J. Adams, M. G. J. Waters, and D. W. Williams, Clin. Oral Implants Res. **17**, 633 (2006).

40. C. Aparicio, A. Padrós, and F.-J. Gil, J. Mech. Behav. Biomed. Mater. **4**, 1672 (2011).

41. N. Gour, K. X. Ngo, and C. Vebert-Nardin, Macromol. Mater. Eng. **299**, 648 (2014).

42. E.-R. Kenawy, S. D. Worley, and R. Broughton, Biomacromolecules **8**, 1359 (2007).

43. G. M. Harbers, K. Emoto, C. Greef, S. W. Metzger, H. N. Woodward, J. J. Mascali, D. W. Grainger, and M. J. Lochhead, Chem. Mater. **19**, 4405 (2007).

44. A. Michelmore, P. Gross-Kosche, S. A. Al-Bataineh, J. D. Whittle, and R. D. Short, Langmuir **29**, 2595 (2013).

45. Y. Li, B. W. Muir, C. D. Easton, L. Thomsen, D. R. Nisbet, and J. S. Forsythe, Appl. Surf. Sci. **288**, 288 (2014).

46. M. Shen, M. S. Wagner, D. G. Castner, B. D. Ratner, and T. A. Horbett, Langmuir **19**, 1692 (2003).

47. V. Zoulalian, S. Zürcher, S. Tosatti, M. Textor, S. Monge, and J.-J. Robin, Langmuir **26**, 74 (2010).

48. A. K. Muszanska, H. J. Busscher, A. Herrmann, H. C. van der Mei, and W. Norde, Biomaterials **32**, 6333 (2011).

49. M. Zhang, T. Desai, and M. Ferrari, Biomaterials 1924 (1998).

50. M. Zhang, T. Desai, and M. Ferrari, Biomaterials **19**, 953 (1998).

51. D. Sakthi Kumar, M. Fujioka, K. Asano, A. Shoji, A. Jayakrishnan, and Y. Yoshida, J. Mater. Sci. Mater. Med. **18**, 1831 (2007).

52. F. Brétagnol, M. Lejeune, A. Papadopoulou-Bouraoui, M. Hasiwa, H. Rauscher, G. Ceccone, P. Colpo, and F. Rossi, Acta Biomater. **2**, 165 (2006).

53. B. Nisol, G. Oldenhove, N. Preyat, D. Monteyne, M. Moser, D. Perez-Morga, and F. Reniers, Surf. Coatings Technol. **252**, 126 (2014).

54. Y. J. Wu, R. B. Timmons, J. S. Jen, and F. E. Molock, Colloids Surfaces B Biointerfaces **18**, 235 (2000).

55. P. Favia, M. Creatore, F. Palumbo, V. Colaprico, and R. d'Agostino, Surf. Coatings Technol. **142-144**, 1 (2001).

56. B. O. Aronsson, J. Lausmaa, and B. Kasemo, J. Biomed. Mater. Res. **35**, 49 (1997).

57. B. Kasemo and J. Lausmaa, J. Biomed. Mater. Res. **22**, 145 (1988).

58. F. Rupp, L. Scheideler, N. Olshanska, M. de Wild, M. Wieland, and J. Geis-Gerstorfer, J. Biomed. Mater. Res. A **76**, 323 (2006).

59. V. S. Smentkowski and C. A. Moore, J. Vac. Sci. Technol. A Vacuum, Surfaces, Film. **31**, 06F105 (2013).

60. W. Petasch, B. Kegel, H. Schmid, K. Lendenmann, and H. . Keller, Surf. Coatings Technol. **97**, 176 (1997).

61. P. Cools, N. De Geyter, E. Vanderleyden, P. Dubruel, and R. Morent, Plasma Chem. Plasma Process. **34**, 917 (2014).

62. B. T. Chaid, N. A. A. Al-Tememee, M. K. Khalaf, and F. T. Ibrahim, Int. J. Recent Res. Rev. **V**, 17 (2013).

63. H. B. Smith, C. Charles, and R. W. Boswell, Phys. Plasmas **10**, 875 (2003).

64. K. T. A. L. Burm, Contrib. to Plasma Phys. **47**, 177 (2007).

65. J. D. Pace and A. B. Parker, J. Phys. D. Appl. Phys. **6**, 1525 (1973).

30

66. R. Schlapak, P. Pammer, D. Armitage, R. Zhu, P. Hinterdorfer, M. Vaupel, T. Frühwirth, and S. Howorka, Langmuir **22**, 277 (2006).

67. S. R. Kane, P. D. Ashby, and L. A. Pruitt, J. Mater. Sci. Mater. Med. **21**, 1037 (2010).

68. E. Johnston, J. Bryers, and B. Ratner, Langmuir 870 (2005).

69. G. Wells, Plasma Process. … **10**, 119 (2013).

70. S. Mutlu, D. Çökeliler, and M. Mutlu, J. Food Eng. **78**, 494 (2007).

71. R. Michel, S. Pasche, M. Textor, and D. G. Castner, Langmuir **21**, 12327 (2005).

72. P. J. Cumpson, Surf. Interface Anal. **29**, 403 (2000).

73. M. Manso, A. Valsesia, M. Lejeune, D. Gilliland, G. Ceccone, and F. Rossi, Acta Biomater. **1**, 431 (2005).

74. A. Roosjen, H. J. Kaper, H. C. van der Mei, W. Norde, and H. J. Busscher, Microbiology **149**, 3239 (2003).

75. G. Da Ponte, E. Sardella, F. Fanelli, A. Van Hoeck, R. d'Agostino, S. Paulussen, and P. Favia, Surf. Coatings Technol. **205**, S525 (2011).

76. G. Da Ponte, E. Sardella, F. Fanelli, R. d'Agostino, R. Gristina, and P. Favia, Plasma Process. Polym. **9**, 1176 (2012).

77. P. Kingshott, J. Wei, D. Bagge-Ravn, N. Gadegaard, and L. Gram, Langmuir **19**, 6912 (2003).

78. Y. Tanaka, K. Matin, M. Gyo, A. Okada, Y. Tsutsumi, H. Doi, N. Nomura, J. Tagami, and T. Hanawa, J. Biomed. Mater. Res. A **95**, 1105 (2010).

31

79. W. J. Yang, T. Cai, K.-G. Neoh, E.-T. Kang, G. H. Dickinson, S. L.-M. Teo, and D. Rittschof, Langmuir **27**, 7065 (2011).